

NAD(P)H: quinone oxidoreductase 1-mediated oxidative stress resistance and tumor microenvironment remodeling in glioblastoma

Yangqing Li[†], Tao Kang[†], Zhen Jia[†], Chenfei Lu[†], Gaoyuan Cui[†], Kefan Song, Hang Yu, Deobrat Dixit, Fangshu Jin, Danyang Shan, Qiankun Lin, Daqi Li, Hao You, Danling Gu, Jiancheng Gao, Zhumei Shi^{ID}, Wei Gao, Fan Lin, Zhe Zhu, Qianghu Wang^{ID}, Weiwei Tao, Junxia Zhang, Jingshan Liang, Zhu Zhu, Yongping You, Xu Qian, Kailin Yang, Xiuxing Wang^{ID}, Jeremy N. Rich^{ID}, Kun Yang, Luan Sun, Chaojun Li^{ID}, and Qian Zhang^{ID}

All author affiliations are listed at the end of the article

Corresponding Authors: Qian Zhang, PhD, National Health Commission Key Laboratory of Antibody Techniques, Department of Cell Biology, Jiangsu Key Laboratory of Molecular Targets and Intervention for Metabolic Diseases, School of Basic Medical Sciences, Nanjing Medical University, Nanjing, Jiangsu 211166, China (zhangqian01@njmu.edu.cn); Chaojun Li, PhD, Ministry of Education Key Laboratory of Model Animals for Disease Study, Model Animal Research Center, Medical School of Nanjing University, National Resource Center for Mutant Mice, Nanjing, Jiangsu 210093, China; State Key Laboratory of Reproductive Medicine and Offspring Health, China International Joint Research Center on Environment and Human Health, Center for Global Health, School of Public Health, Gusu School, Nanjing Medical University, Nanjing, Jiangsu 211166, China (lichaojun@njmu.edu.cn).

[†]These authors contributed equally to this work.

Abstract

Background. Glioblastoma (GBM) is a highly aggressive brain tumor, with glioblastoma stem cells (GSCs) occupying the pinnacle of a complex tumor microenvironment (TME), conferring therapeutic resistance. The TME plays a role in tumor development by creating a niche rich in reactive oxygen species (ROS) through oxidative stress (OS). Here, we identified NAD(P)H: quinone oxidoreductase 1 (NQO1) as an essential regulatory factor in antioxidant stress response, which is key to maintaining GSCs and the immunosuppressive TME.

Methods. Proteomics analysis and epigenetic profiling using H3K27ac ChIP-sequencing and single-cell RNA sequencing were performed to define the high enrichment of *NQO1* in GBM. In vitro and in vivo loss-of-function genetic and pharmacologic assays were conducted to evaluate the effect of NQO1 in GSC proliferation and self-renewal. Patient-derived GSCs and xenograft murine models were used to investigate the tumor-intrinsic and extrinsic mechanisms that confer resistance to OS and reprogram the immunosuppressive TME.

Results. *NQO1* was preferentially expressed in GSCs and regulated ROS levels, preserving the stability of nuclear Lamin B1 and inhibiting cGAS-type I interferon signaling, which helps to remodel the immunosuppressive TME. Furthermore, nuclear factor erythroid 2-related factor 2 (NRF2) transcriptionally regulates NQO1, suppressing type I interferon signaling.

Conclusions. NQO1 plays critical roles at both the cell-autonomous and cell-extrinsic levels for clinical treatment. Targeting NQO1 and its downstream signaling pathways, including β -lapachone and immune checkpoint inhibitors such as anti-PD-1 therapy, enhances our understanding of the interactions between GSCs, OS, and the TME. This offers promising new avenues for clinical intervention in GBM.

Key Points

- In glioblastoma, NAD(P)H: quinone oxidoreductase 1 (NQO1) is essentially consistent with the enrichment of reactive oxygen species (ROS).
- NQO1 promotes glioblastoma stem cell proliferation and self-renewal.
- NQO1 resists oxidative stress and remodels tumor microenvironment through ROS-Lamin B1 axis.

Received June 2, 2025; accepted January 16, 2026.

© The Author(s) 2026. Published by Oxford University Press on behalf of the Society for Neuro-Oncology. All rights reserved. For commercial re-use, please contact reprints@oup.com for reprints and translation rights for reprints. All other permissions can be obtained through our RightsLink service via the Permissions link on the article page on our site—for further information please contact journals.permissions@oup.com.

Importance of the Study

NAD(P)H: quinone oxidoreductase 1 (NQO1) serves as both an antioxidant stress response regulator and a factor in maintaining glioblastoma stem cells within an immunosuppressive tumor microenvironment (TME). NQO1 prevents oxidative stress by reducing reactive oxygen species levels, which supports the stability of nuclear

Lamin B1 and further inhibits cGAS-STING signaling and type I interferon pathways, contributing to the remodeling of the immunosuppressive TME. Targeting NQO1 and its downstream signaling effectors, such as β -lapachone and immune checkpoint therapy with anti-PD-1, offers effective strategies for treating glioblastoma.

Glioblastoma (GBM) is an invariably aggressive tumor of the central nervous system for which no curative treatment is currently available.^{1,2} Despite adherence to the standard-of-care protocols encompassing maximal surgical resection, concurrent radiotherapy, and adjuvant therapy with the oral alkylating agent temozolomide, the prognosis for individuals with glioblastoma multiforme remains poor, with a median survival of less than 2 years.^{3,4} Glioblastoma stem cells (GSCs) are a small subpopulation of tumor cells exhibiting the fundamental features of stem cells, including self-renewal, differentiation, and tumor initiation capability.⁵ GSCs represent a neoplastic cell population that resides at the apex of the cellular hierarchy, endowing with a profound resistance to conventional therapy.⁶

Glioblastoma stem cells thrive in the intricate tumor microenvironment (TME), unaffected by the stringent regulatory mechanisms that typically restrict the proliferation and survival of their nonmalignant counterparts.⁷ The glioblastoma TME comprises a diverse array of nonneoplastic cells, encompassing both infiltrating and resident immune constituents and vascular elements such as endothelial and pericyte cells.⁸ The immunosuppressive cells, including tumor-associated macrophages and microglia (TAMs), myeloid-derived suppressor cells (MDSCs), and regulatory T cells, act in concert within the TME to promote immunosuppression and facilitate immune evasion by tumor cells.^{9,10} Given the pivotal role of GSCs and crosstalk with the TME, targeting GSCs and their interactions with TME components has the potential to improve GBM treatment.

Oxidative stress (OS) is a condition caused by exposure to deleterious endogenous or exogenous stimuli or by oxidant-antioxidant imbalance.¹¹ Elevated levels of OS can increase reactive oxygen species (ROS) within cells, which causes DNA damage, protein oxidation, and lipid peroxidation.^{12,13} Tumor cells enhance antioxidant capacity to optimize ROS-driven proliferation avoiding senescence or apoptosis.¹⁴ GBM exhibits a strong association with OS due to the elevated cerebral oxygen metabolism.¹⁵ Severe OS in microglia induces NR4A2-dependent transcription, dysregulating cholesterol homeostasis, and fostering an immunosuppressive TME.¹⁶ ROS drives GBM progression through mitochondrial dysfunction, impaired DNA repair, metabolic reprogramming, and mTORC1-mediated M2 macrophage polarization.^{17,18} However, the elevated ROS against OS in the interplay between GSCs and immune cells remains underexplored.

NAD(P)H: quinone oxidoreductase 1 (NQO1) serves as a cytosolic enzyme that converts quinone-based prodrugs to hydroquinone, preventing OS, ROS generation, and carcinogenesis.^{19,20} NQO1 is markedly elevated in various cancers,

and its high expression has been associated with shorter survival in GBM.^{21,22} NQO1 promotes GBM aggressiveness through epithelial-mesenchymal transition induction via the PI3K/AKT/mTOR/Snail pathway.²³ Transcription of NQO1 mediated by C/EBP β neutralizes ROS and promotes GBM survival,²⁴ but the underlying mechanisms in GSCs and their TME remain elusive. Here, we provide evidence that NQO1 contributes to GSC proliferation and self-renewal and explore how NQO1 supports GSCs and remodels the TME. This study reveals new therapeutically available targets at the cell-autonomous and cell-extrinsic levels for clinical treatment.

Methods

Culture of Patient-Derived GSCs and Cell Lines

Glioblastoma stem cell tissues were obtained from excess surgical resection samples of patients who were treated at Case Western Reserve University, following review by the neuropathology department and with appropriate patient consent, in accordance with an Institutional Review Board-approved protocol (protocol number 090401). Patient-derived xenografts were established and maintained as a renewable source of GSCs, minimizing in vitro artifacts associated with cell culture. Authentication of tumor models was conducted using short tandem repeat analysis. GSCs were isolated and sorted as CD133⁺ cells using CD133 antibody-conjugated magnetic beads (Miltenyi Biotec). Expression of stem cell markers, functional assays of self-renewal and tumor propagation were used to validate GSC phenotypes as previously described.^{25–27} GSCs were cultured as neurospheres in Neurobasal medium (Invitrogen) supplemented with B27 supplement without vitamin A (Life Technologies), Glutamax (Life Technologies), sodium pyruvate (Life Technologies), penicillin/streptomycin, 20 ng/mL EGF and basic fibroblast growth factor (bFGF, R&D Systems) at 37°C with 20% oxygen and 5% carbon dioxide. Matched differentiated glioblastoma cell (DGC) populations were induced by Dulbecco's Modified Eagle Medium (DMEM, HyClone) supplemented with 10% fetal bovine serum (FBS, Sigma) to maintain differentiation status.

The nonmalignant neural stem cell models, ENSA and HNP1, were utilized in this study. ENSA (ENStem-A) is a human embryonic stem cell-derived neural progenitor (Millipore Sigma, Cat# SCC003). HNP1 (STEMEZ HNP1) is a human neural progenitor cell line (Neuromics, Cat# HN60001). 293T cells (ATCC, Cat# CRL-3216) were used to

produce lentiviral particles. CT-2A cells (Sigma-Aldrich, SCC194) were used for intracranial tumor formation in mice.

In Vivo Tumorigenesis and Animal Models

All BALB/c-Nude (female, 4-week-old) and C57BL/6J (female, 5-week-old) mice were obtained from Jiangsu GemPharmatech Co., Ltd and raised under specific pathogen-free conditions at Animal Center of Nanjing Medical University (ethical approval: IACUC-2006033-2) per NIH and institutional guidelines. Animals were randomly assigned to experimental groups. Intracranial xenograft models were established by implanting 5×10^4 patient-derived GSCs (839 and 2907) or 2×10^5 CT-2A cells into the cerebral cortex of mice. Postoperative monitoring included twice-daily clinical assessments for neurological deficits (ataxia and seizures) or humane endpoints, with prompt euthanasia via cervical dislocation under deep anesthesia upon criteria fulfillment. Tumor progression was longitudinally tracked using an IVIS Spectrum imaging system following weekly intraperitoneal administration of D-Luciferin potassium salt (150 mg/kg). All procedures adhered to Nanjing Medical University's Institutional Animal Care Guidelines and the 3R principles.

Proliferation and Neurosphere Formation Assays

CellTiter-Glo assay (Promega) was used to quantify cell proliferation. GSCs were seeded into 96-well plates at a density of 2000 cells per well (6 replicates per group). Cellular viability was measured at 1, 3, 5, and 7 days. Data were normalized to day 1 and presented as mean \pm SD. The number of neurospheres and cell numbers in each well were recorded 7 days after plating. For extreme limiting dilution analysis, cells were plated as gradient concentrations (1, 3, 15, 30, 60, and 150 cells per well).²⁶ Extreme limiting dilution analysis was conducted via extreme limiting dilution algorithms using the online ELDA platform <http://bioinf.wehi.edu.au/software/elda>.²⁸

Plasmids and Lentiviral Transduction

All shRNAs used were obtained from Sigma-Aldrich and were listed in [Supplementary Table S1](#). Non-overlapping shRNAs (Sigma-Aldrich, SHC002) were selected based on knockdown efficiency and used for all following experiments. Lentiviral particles were generated in 293T cells in DMEM medium containing 10% fetal bovine serum with co-transfection with the packaging vectors psPAX2 and pMD2.G (Addgene) using a standard calcium phosphate transfection method in neurobasal complete medium.

RNA Isolation and Quantitative RT-PCR

Total cellular RNA from cells was isolated by RNAiso Plus (Takara). The PrimeScript cDNA Synthesis Kit (Takara) was used for reverse transcription into cDNA. qRT-PCR was performed using the Applied Biosystems Stepone Plus cycler

with ChamQ SYBR qPCR Master Mix (Vazyme). The sequences of primers used in this study are listed in [Supplementary Table S1](#).

Immunoblotting

Cells were collected and lysed in RIPA buffer (50 mM Tris-HCl pH 7.5, 150 mM NaCl, 0.5% NP-40, 0.1% SDS, and supplemented with protease inhibitors and phosphatase inhibitors), then incubated on ice for 30 minutes. Lysates were centrifuged at 4°C for 10 minutes at 12 000 rpm. Supernatants were subjected to SDS-PAGE and transferred to polyvinylidene difluoride membranes (Millipore). The membranes were blocked with 5% nonfat milk for 1 hour and immunoblotted with primary antibodies overnight at 4°C, followed by the HRP-conjugated antibody at room temperature for 1 hour. Proteins were detected with antibodies against NQO1 (Cell Signaling, 3187S, Abcam, ab80588), β -Tubulin (Abcepta, AM1031A), SOX2 (Cell Signaling, 3579, Proteintech, 66411-1-Ig), OLIG2 (Sigma-Aldrich, MABN50), Flag-Tag (Cell Signaling, 14793S), Lamin B1 (Proteintech, 66095-1-Ig), LC3B (Cell Signaling, 2775S), TBK1 (Cell Signaling, 3504S), p-TBK1 (Cell Signaling, 5483S), cGAS (Cell Signaling, 15102S), STING (R&D, MAB7169), p-STING (Cell Signaling, 19781S), nuclear factor erythroid 2-related factor 2 (NRF2) (Affinity, AF0639). Antibody validation was performed per the manufacturer's instructions.

Immunofluorescence

Cells were plated on matrigel-coated coverslips and fixed 24 hours later with 4% paraformaldehyde for 20 minutes, then washed 3 times with PBS. Permeabilization was conducted with 0.30% Triton X-100 for 15 minutes, followed by blocking in 3% bovine serum albumin at room temperature for 2 hours. Immunostaining was conducted using primary antibodies against SOX2 (R&D, MAB2018), NQO1 (Proteintech, 11451-1-AP, CST, 3187S), CD133 (Proteintech, 66666-1-Ig), Lamin B1 (Proteintech, 66095-1-Ig), cGAS (Cell Signaling, 15102S), and double-strand DNA (dsDNA) (Abcam, AB27156), which were incubated overnight at 4°C, followed by secondary antibodies at room temperature. Nucleus was stained with DAPI for 5 minutes at room temperature. Images were captured using a Zeiss LSM770 microscope (Carl Zeiss).

Co-Immunoprecipitation

Glioblastoma stem cells were collected and lysed in IP buffer (20 mM Tris-HCl, 150 mM NaCl, 1% Triton X-100, 0.5% sodium deoxycholate, 1 mM DTT) containing PMSF and cocktail protease inhibitor at 4°C, followed by centrifugation at 12 000 g for 10 minutes at 4°C, and supernatants were collected. The antibody of anti-NQO1 (Proteintech, 11451-1-AP) of nonspecific IgG (Beyotime, A7016) was added to the supernatants and incubated at 4°C overnight. The supernatants were immunoprecipitated by incubation with Protein A/G sepharose beads (Beyotime) at 4°C for 4 hours followed by washing beads together with captured proteins.

Chromatin Immunoprecipitation

The SimpleChIP Enzymatic Chromatin IP Kit (Cell Signaling, #9003) was utilized for chromatin immunoprecipitation. A total of 4×10^6 cells per group were collected, and crosslinking was initiated by adding formaldehyde, followed by the addition of 10× glycine at room temperature for 5 minutes. The precipitation was collected after centrifugation at 1500 rpm for 5 minutes at 4°C, and chromatin clipping was performed according to the kit protocol. Chromatin immunoprecipitation (ChIP) was performed by adding the specific antibody anti-NRF2 (Cell Signaling, 12721S) at 4°C and incubating overnight after measuring the chromatin concentration. Magnetic beads were added to the chromatin-protein crosslink solution and incubated for 4 hours. The chromatin was eluted and uncross-linked from the magnetic beads by incubating for 4 hours at 65°C, followed by digestion with proteinase K. The collected DNA was subsequently analyzed using qPCR. A complete list of all primers used can be found in [Supplementary Table S1](#).

Proteomics Sequencing and Data Analysis

Neural stem cells (NSCs) and GSCs in logarithmic growth phase were enzymatically dissociated and quantified to 5×10^6 cells with PBS washing, followed by flash-freezing in liquid nitrogen for proteomic analysis conducted by Hangzhou Jingjie Biotechnology Co., Ltd (China) through RIPA-based protein extraction, LC-MS/MS, and MaxQuant (v1.6.6.0) analysis against UniProtKB Homo sapiens database, with differential proteins identified using adjusted $P < .05$ and fold change thresholds (>1.5 for upregulation, $<1/1.5$ for downregulation).

RNA Sequencing and Data Analysis

Total RNA was extracted with RNAiso Plus (Takara). RNA sequencing was performed using BGISEQ-500 platforms. FASTQ sequencing reads were trimmed using Trim Galore (RRID: SCR_011847), and transcript quantification was conducted using Salmon with the quasi-mapping mode.²⁹ Salmon “quant” files were converted using Tximport,³⁰ and differential expression analysis was performed using DESeq2.³¹ Gene set enrichment analysis was performed by selecting differentially expressed genes (FDR-corrected P -value $< .05$), generating a preranked list, and importing the preranked list into the GSEA desktop application (<http://www.gsea-msigdb.org/gsea/index.jsp>).

Spatial Transcriptomics Analysis

A cohort of 3 newly diagnosed isocitrate dehydrogenase wild-type (IDH-WT) glioblastoma multiforme (GBM) samples was analyzed with SPATA2.³² Scaled gene expression values (to plot single genes) or enrichment scores of a defined gene set were utilized for spatial expression plots. Spatial coordinates corresponding to hematoxylin and eosin-stained histological sections were assigned through input files, with x-axis and y-axis positions mapped to tissue localization.

The data were illustrated as surface plots (plotly package R-software).

Single-Cell Sequencing Analysis

The single-cell RNA sequencing data analyzed in this study were derived from the publicly available dataset GSE182109 deposited in the Gene Expression Omnibus (GEO) repository. The single-cell RNA sequencing data were analyzed using Cell Ranger pipeline (v6.1.2, 10X Genomics) with default alignment parameters against the GRCh38 human reference genome. Subsequent quality control and analytical workflows were implemented through the Seurat package (v4.3.0).

ROS Detection

The ROS-Glo H_2O_2 assay (Promega) kit was used to detect the level of ROS. Cells were seeded into 96-well plates at 2000 cells per well (6 replicates per group). Each well was supplemented with substrate to achieve a final substrate concentration of 25 μ M, followed by incubation at 37°C, 5% CO_2 for 6 hours. Subsequently, ROS-Glo detection reagent was added for light-protected incubation for 20 minutes. Luminescence signals were quantified using a microplate reader (BioTek). All experimental data were normalized to vehicle controls and expressed as mean \pm SD.

Type I IFN Measurement

IFN α and IFN β levels in GSC culture supernatants were detected by Human IFN α ELISA kit (Elabscience, E-EL-H6125) or Human IFN β ELISA kit (Elabscience, E-EL-H0085) following the manufacturer's instructions. The absorbance was measured at a wavelength of 450 nm. Data were presented as mean \pm SD.

Flow Cytometry

To quantify immune cells in xenograft-bearing mice, we dissected brain tumors, and digested with 5 mg/mL Collagenase (Gibco, 17104-019) and 0.1 mg/mL DNase (Sigma-Aldrich, DN25) for 30 minutes. Immune cells were separated by 30% and 70% percoll (Cytiva, 17089101) gradients at 700 g for 30 minutes. The remaining cells were suspended in 2% BSA and stained with FVS780 (BD, 565388), followed by blocking with Mouse Fc Block (BD, 553141). Cells were then stained with anti-CD45 (BD, 563890), anti-CD3 (BD, 553061, 563565), anti-CD4 (BD, 563232), anti-CD8 (BD, 552877), anti-CD11b (BD, 557396), anti-CD25 (BD, 561065), anti-F4/80 (BD, 743282), and anti-GR1 (BD, 553126) for 30 minutes. After permeabilized for 40 minutes, cells were stained with anti-FOXP3 (Invitrogen, 17-5773-82) and anti-IFN- γ (BioLegend, 505838) for 30 minutes. Splenocytes were stained and examined by flow cytometry to identify the immune microenvironment of xenograft GBM in mice.

Glioblastoma stem cells and non-GSC tumor cells of GBM patient samples were isolated and stained with FVD777

(STARTER, S0D0026), anti-CD45 (BD, 555482), anti-CD133 (BioLegend, 397905, Invitrogen, 12-1338-42), anti-CD147 (BioLegend, 306211). Then CD133⁺CD147⁺ GSCs and CD133⁺CD147⁻ non-GSC tumor cells were sorted by flow cytometry for further study. The data were analyzed with FlowJo v.10.

Statistical Analysis

All numerical data are presented as the mean \pm SD from at least 3 independent experiments. Statistical analyses were conducted using GraphPad Prism with Student's *t*-test or ANOVA as appropriate. The statistical differences between groups for Kaplan-Meier survival curves were determined using the log-rank test. Blinding and randomization were applied in all experiments. The correlation between gene expression and patient survival was analyzed through brain tumor datasets sourced from The Cancer Genome Atlas (TCGA), Gravendeel, and LeeY, which were downloaded from the TCGA data portal or the National Center for Biotechnology Information GEO database.

Results

Enrichment of ROS and Preferential Expression of NQO1 in GSCs

To identify proteins differentially expressed and specific to GSC-mediated GBM progression, we performed proteomics analysis of patient-derived GSCs compared with NSCs. We identified NQO1 as the solitary factor with the largest fold change between GSCs and NSCs (fold change > 1.5) (Figure 1A). Furthermore, we interrogated the epigenetic profile of NQO1 using H3K27ac ChIP-seq data and observed an activation of the promoter regions surrounding the NQO1 locus in GSCs (Figure 1B, Supplementary Figure S1A). We interrogated single-cell RNA sequencing data (Figure 1C, Supplementary Figure S1B) and observed the high enrichment of NQO1 in GSC-like tumor cells. We observed an 88.86% overlap between NQO1 expression and SOX2-positive cells in single-cell RNA sequencing data, indicating that NQO1 is expressed explicitly in stem-like populations (Figure 1C). We thus hypothesized that NQO1 is preferentially expressed in GSCs. Quantitative reverse transcription (RT)-PCR and immunoblot analysis confirmed that the expression level of NQO1 was significantly elevated in GSCs compared to NSCs (Figure 1D and E). Immunofluorescent staining with NQO1 and the GSC marker SOX2 or CD133 confirmed that NQO1 was enriched in patient-derived GSCs (839, 2907, 3028, RKI, and MES28) compared with NSCs (ENSA and HNP1) (Figure 1F, Supplementary Figure S1C). Further, we analyzed the high correlation between NQO1 and the ROS pathway by utilizing data from the TCGA GBM dataset and RNA sequencing derived from 41 GSCs and 5 NSCs (Figure 1G). By analyzing GBM spatial transcriptomics and spatial trajectory analysis, we found that the expression of NQO1 is essentially consistent with the distribution of ROS (Figure 1H, Supplementary Figure S1D-F). Further, we exposed GSCs (839, 2907, 3028, MES28, RKI) and NSCs (ENSA, HNP1) to hydrogen peroxide (H₂O₂)-induced OS and found that the

GSCs exhibited lower sensitivity compared with NSCs (Figure 1I). In addition, GSCs exhibited higher resistance to tert-butyl hydroperoxide (TBHP)-induced OS than NSCs (Supplementary Figure S1G). In matched pairs of GSCs and differentiated GBM cells (DGCs) (839, 2907, 3028, MES28, RKI), we found that GSCs expressed higher levels of NQO1 (Supplementary Figure S2A-C) and exhibited lower sensitivity to H₂O₂- and TBHP-induced OS than DGCs (Figure 1J, Supplementary Figure S2D and E). Furthermore, we isolated GSCs and non-GSCs with stem cell marker CD133 and the malignant cell marker CD147 from the GBM patient samples, immunoblotting confirmed that the GSCs (CD133⁺CD147⁺) exhibited markedly higher NQO1 expression compared to non-GSC tumor cells (CD133⁺CD147⁻) (Supplementary Figure S2F and G). Collectively, these data demonstrate that NQO1 is preferentially expressed in GSCs, suggesting that it may contribute to GBM pathology by protecting against OS.

NQO1 Is Essential for GSC Proliferation and Self-Renewal

To investigate the role of NQO1 in promoting GSC proliferation and self-renewal, we performed loss-of-function and overexpression studies in our patient-derived GSC models. Silencing NQO1 using 2 nonoverlapping short hairpin RNAs (shRNA) in 2 GSC models (839 and 2907 GSCs) reduced the mRNA and protein levels of NQO1 in GSCs (Figure 2A and B). Knockdown of NQO1 decreased GSC proliferation and self-renewal ability, as measured by reduced cell viability, neurosphere formation capability, cell number, and in vitro limiting dilution assays (Figure 2C-G, Supplementary Figure S3A). Additionally, overexpression of NQO1 promoted GSC proliferation and self-renewal (Supplementary Figure S3B-D). To establish the effect of NQO1 knockdown in GSCs, we reconstituted the NQO1 expression in NQO1-knockdown cells, restoring the decreased cell viability of GSCs (Supplementary Figure S3E-G). NQO1 targeting using shRNA transduction reduced the mRNA and protein levels of the GSC markers, SOX2 and OLIG2 (Supplementary Figure 3H and I).

To validate the in vivo function of NQO1 in tumor propagation of GSCs. We transplanted the GSCs (839 and 2907) transduced with shRNAs into the brains of immunocompromised mice. Mice bearing GSCs transduced with shNQO1 displayed prolonged survival and reduced tumor volumes compared with those bearing GSCs transduced with shCONT (Figure 2H-J, Supplementary Figure S3J-M). These data support the biological function of NQO1 in supporting GSC maintenance.

NQO1 Confers Resistance to Oxidative Stress and Promotes the Maintenance of the Nuclear Lamin B1 in GSCs

To identify the downstream mechanisms and targets of NQO1 in maintaining GSCs, we performed immunoprecipitation followed by mass spectrometry using an anti-NQO1 antibody from cell lysates derived from 2 patient-derived GSCs. By combining mass spectrometry data with NQO1-correlated proteins in 839 and 2907 GSCs, the nuclear

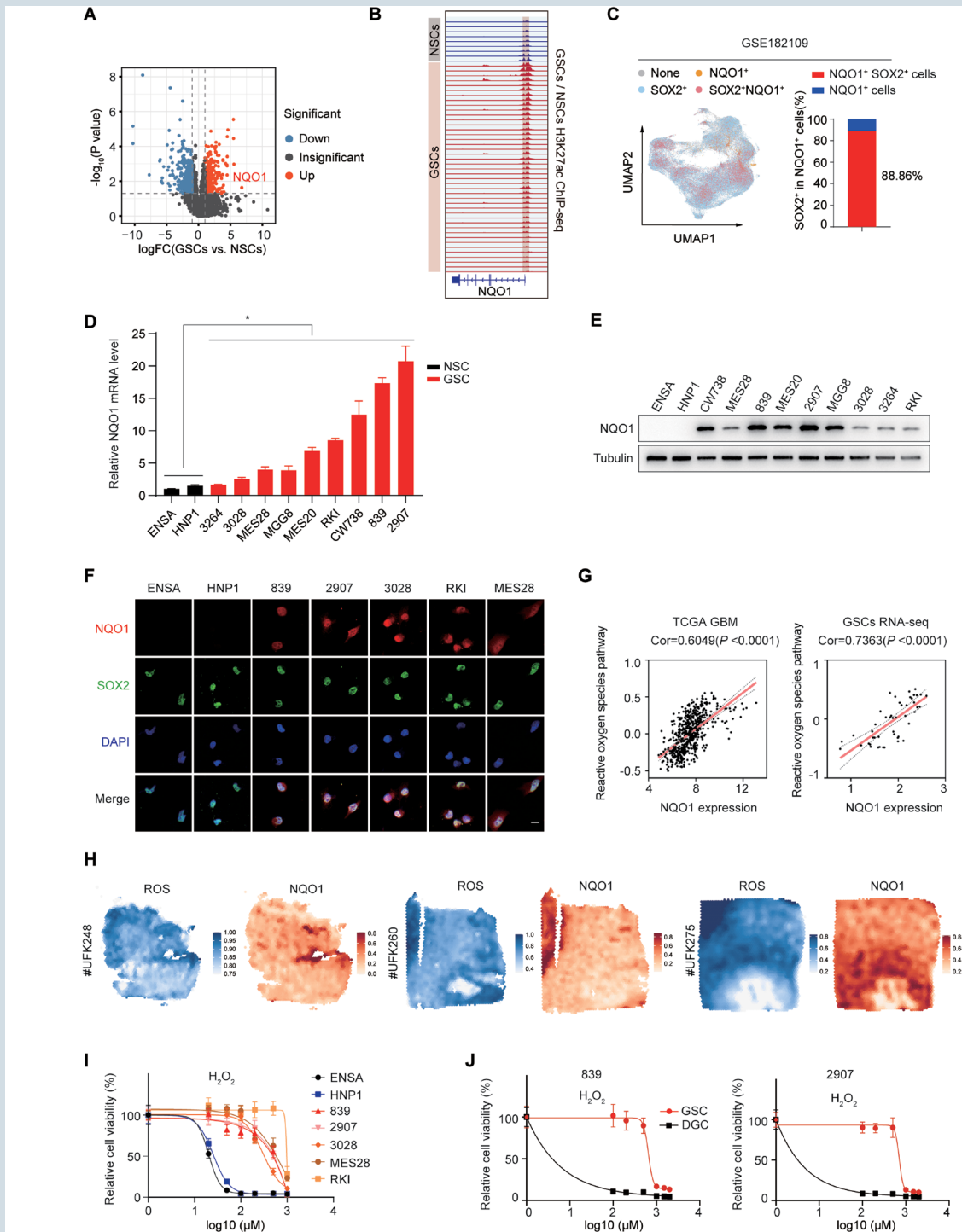


Figure 1. Enrichment of reactive oxygen species (ROS) and preferential expression of NAD(P)H:quinone oxidoreductase 1 (NQO1) in glioblastoma stem cells (GSCs). (A) Volcano plot illustrates the differentially expressed proteins in GSCs ($n=8$) compared to NSCs ($n=2$) by proteomics sequencing, with a P value $< .05$.³³ (B) Representative image of ChIP-seq data (GSE119776) showing H3K27ac levels at the promoter region surrounding the NQO1 gene locus in GSCs.³⁴ (C) The UMAP plot of GBM tumor cells is annotated by the overlap of NQO1 and SOX2 positive cells, analyzed using single-cell RNA sequencing data from the GEO database (GSE182109). (D) Quantitative RT-PCR of NQO1 mRNA levels in GSCs ($n=9$) and NSCs ($n=2$). Data are determined by unpaired t test and presented as the mean \pm SD. * $P < .05$. (E) Protein levels of NQO1 in GSCs ($n=9$) and NSCs ($n=2$) were measured using western blot analysis. (F) Immunofluorescence image of NQO1 and SOX2 expression in GSCs and NSCs. Scale bar, 10 μm . (G) The correlation between NQO1 expression and the ROS pathway in the TCGA GBM database and RNA sequencing data from GSCs. (H) Gene expression surface plots illustrate the spatial transcriptomics overlap of NQO1 and ROS pathway expression.³⁵ (I) Dose-response curves for H₂O₂ stimulation were generated for GSCs ($n=5$) and NSCs ($n=2$), as measured by a CellTiter-Glo assay. Data are presented as mean \pm SD from 6 independent experiments. (J) Dose-response curves for H₂O₂ stimulation were generated for GSCs and matched DGCs, as measured by a CellTiter-Glo assay. Data are presented as mean \pm SD from 6 independent experiments.

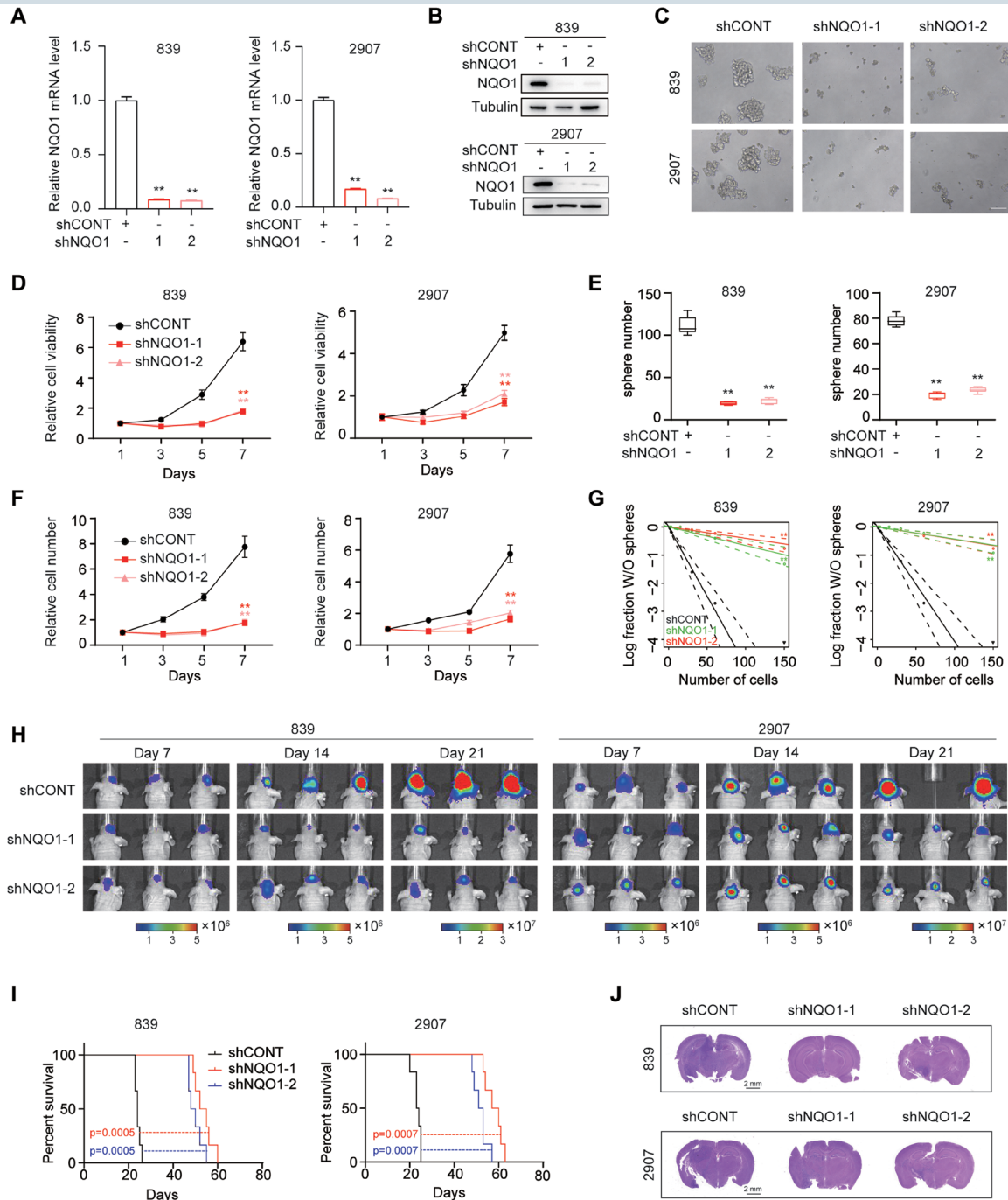


Figure 2. NAD(P)H: quinone oxidoreductase 1 (NQO1) is essential for glioblastoma stem cell (GSC) proliferation and self-renewal. (A) Quantitative RT-PCR of *NQO1* mRNA levels in 839 and 2907 GSCs expressing a nontargeting control shRNA (shCONT) or *NQO1*-specific shRNA (shNQO1-1 and shNQO1-2). Data were determined by unpaired t test and presented as the mean \pm SD. ** $P < .01$. (B) Protein levels of NQO1 were assessed in 839 and 2907 GSCs following transduction with 2 independent shRNAs (shNQO1-1 and shNQO1-2) compared to the control (shCONT). (C) Representative images of neurospheres derived from 839 and 2907 GSCs expressing shCONT, shNQO1-1, or shNQO1-2. Scale bar, 100 μ m. (D) Relative cell viability of 839 and 2907 GSCs expressing shCONT, shNQO1-1, or shNQO1-2, as measured by a CellTiter-Glo assay. Data are presented as mean \pm SD from 6 independent experiments. ** $P < .01$. (E) Quantification of the sphere number formed by 839 and 2907 GSCs expressing shCONT, shNQO1-1, or shNQO1-2. ** $P < .01$. (F) Quantification of the cell number formed by 839 and 2907 GSCs expressing shCONT, shNQO1-1, or shNQO1-2. ** $P < .01$. (G) Extreme limiting dilution assays (ELDA) indicated that the knockdown of *NQO1* in 839 and 2907 GSCs reduced sphere formation. ** $P < .01$. (H) In vivo bioluminescent imaging of tumor growth was performed in nude mice bearing glioblastoma xenografts derived from 839 and 2907 GSCs expressing shCONT, shNQO1-1, or shNQO1-2 on days 7, 14, and 21. (I) Kaplan-Meier survival curves for nude mice with glioblastoma xenografts derived from 839 and 2907 GSCs expressing shCONT, shNQO1-1, or shNQO1-2 ($n = 6$). P -values were determined using the log-rank test. (J) Representative images of hematoxylin and eosin staining of mouse brain tissue collected on day 21 after transplantation of 839 and 2907 GSCs expressing shCONT, shNQO1-1, or shNQO1-2. Scale bar, 2 mm.

lamina proteins, including Lamin B2 and Lamin B1, were identified as the top 4 ranked NQO1-correlated proteins (Figure 3A and B, Supplementary Figure S4A). Silencing *LMNB1* in 839 and 2907 GSCs resulted in significantly reduced cell viability compared to silencing *LMNB2* (Figure 3C). Considering the OS-associated function, we treated 839 and 2907 GSCs with H₂O₂-induced OS, comparing the effects of knockdown of *LMNB1* or *LMNB2* to those of shCONT, observing that knockdown of *LMNB1* under H₂O₂-induced OS markedly reduced cell viability compared with that of silencing *LMNB2* (Supplementary Figure S4B). Treatment with the antioxidant N-acetylcysteine (NAC) restored Lamin B1 protein levels substantially more than Lamin B2 levels under H₂O₂ exposure, indicating that Lamin B1 is more susceptible to H₂O₂-induced OS (Supplementary Figure S4C). Co-immunoprecipitation and confocal imaging confirmed the interaction of NQO1 and Lamin B1 in 839 and 2907 GSCs (Figure 3D and E). Silencing *NQO1* decreased the expression level of Lamin B1 but elevated the ROS level and the GSCs sensitivity to H₂O₂-induced OS (Figure 3F and G, Supplementary Figure S4D). Overexpression of *NQO1* attenuated *NQO1* silencing-induced ROS accumulation (Figure 3H). Treatment with NAC restored Lamin B1 expression following *NQO1* silencing without affecting *NQO1* expression, demonstrating that NQO1 maintains Lamin B1 expression through ROS suppression (Figure 3I). To investigate the mechanism underlying NQO1-mediated Lamin B1 expression, analysis of TCGA GBM datasets revealed an inverse correlation between *NQO1* expression and autophagic response (Figure 3J, Supplementary Figure S4E). The autophagy-dependent degradation of Lamin B1 involves coordinated regulation by LC3 isoforms, with membrane-conjugated LC3-II serving as the principal operational marker.³⁶ During autophagosome biogenesis, LC3 undergoes phosphatidylethanolamine conjugation (LC3-I to LC3-II transition), with LC3-II specifically localizing to autophagosomal membranes to mediate membrane expansion and maturation.³⁷ Then we performed co-immunoprecipitation assay and confirmed the interaction of Lamin B1 and LC3 in 839 and 2907 GSCs. Knocking down of *NQO1* reduced the interaction of Lamin B1 with LC3 but increased the protein level of LC3 II (Figure 3K). Thus, we hypothesize that NQO1 maintains Lamin B1 stabilization by attenuating its autophagic degradation via LC3-mediated recognition. Under H₂O₂-induced OS, *NQO1* silencing promotes Lamin B1 degradation while concomitantly elevating lipidated LC3-II levels (Figure 3L, Supplementary Figure S4F), suggesting that NQO1-mediated stabilization of nuclear Lamin B1 via autophagic suppression. Collectively, these results establish that NQO1 confers OS resistance through ROS inhibition while preserving nuclear Lamin B1 stability in GSCs by suppressing the autophagy pathway.

NQO1 Inhibits cGAS- Type I Interferon Signaling

To further investigate the downstream signaling of NQO1, which induces OS resistance and promotes the maintenance of Lamin B1, we targeted *NQO1* expression in GSCs and performed RNA sequencing to assess alterations in downstream transcriptional networks. Hallmark enrichment and GSEA analysis revealed that Interferon Alpha response signaling was one of the most altered pathways following

NQO1 knockdown in GSCs, *NQO1* expression is negatively correlated with the gene set responding to type I interferon signaling (Figure 4A and B). RNA sequencing data demonstrated that silencing *NQO1* induces the upregulation of the downstream type I interferon signaling-associated genes (Figure 4C). Confocal microscopy observed that silencing *NQO1* or *LMNB1* revealed that the dsDNA released into the cytoplasm as evidenced by the emergence of cytosolic dsDNA, suggesting compromised nuclear integrity (Figure 4D). As our findings that NQO1 induced OS resistance and promoted the maintenance of the nuclear Lamin B1, we hypothesize that inhibiting NQO1 activates OS and causes the degradation of Lamin B1, which activates the downstream cGAS-type I interferon signaling. Immunoblotting verified that genetic targeting *NQO1* or *LMNB1* upregulated the cGAS-STING signaling as measured by the protein level of pTBK1, cGAS, and pSTING (Figure 4E). The DNA chromatin released into the cytoplasm may result in the cGAS-STING signaling stimulation and type I interferon production enhancement. Next, we explored that loss of *NQO1* increased the gene levels of IFN signaling in GSCs, such as *DHX58*, *GBP2*, *IFIH1*, *IL7*, and *TXNIP* (Figure 4F, Supplementary Figure S5A). ELISA assays verified the increased levels of interferon alpha and interferon beta production in 839 or 2907 GSC supernatant after knocking down *NQO1* in GSCs (Figure 4G and H). Therefore, these data suggested that NQO1 maintains nuclear Lamin B1 integrity and inhibits cGAS-STING and type I interferon signaling.

NRF2 Transcriptionally Regulated NQO1 Inhibits cGAS-STING Signaling

To further investigate the mechanisms that mediate *NQO1* expression, we analyzed the binding sites of GBM/GSC-related transcription factors in the promoter region of *NQO1* in transcription landscapes of patient-derived GBM cells. *NQO1* displayed active sites for the nuclear factor erythroid 2-related factor 2 (NRF2, encoded by *NFE2L2*). *NFE2L2* expression is significantly higher in GBM tissues compared to non-tumor tissues, as demonstrated in the TCGA GBM dataset. And *NFE2L2* portends poor prognosis in patients with glioblastoma (Figure 5A). To directly confirm *NFE2L2* binding on the *NQO1* promoter in GSCs, we performed ChIP with an NRF2 antibody, followed by qPCR with primer sets designed for the promoter region of *NQO1*. *NFE2L2* indeed occupied the promoter region of *NQO1*, as evidenced by the comparison with control IgG (Figure 5B and C). NRF2 is preferentially expressed in GSCs compared with NSCs (ENSA, HNP1) (Figure 5D). Silencing *NFE2L2* markedly decreased the gene and protein level of NQO1 (Figure 5E-G). To detect whether NRF2 regulated downstream cGAS-STING signaling, we observed that loss of *NFE2L2* decreased NQO1, Lamin B1, and activated the phosphorylation level of pTBK1 and pSTING. Overexpression of *NQO1* rescued Lamin B1 and inhibited the increased level of cGAS, pTBK1, and pSTING subjected to *NFE2L2* silencing (Figure 5H). However, overexpression of *LMNB1* cannot rescue NQO1 but inhibits the increased level of downstream cGAS, pTBK1, and pSTING subjected to *NFE2L2* silencing. Treatment with antioxidant NAC increased Lamin B1 expression and inhibited the cGAS-STING signaling (Figure 5I).

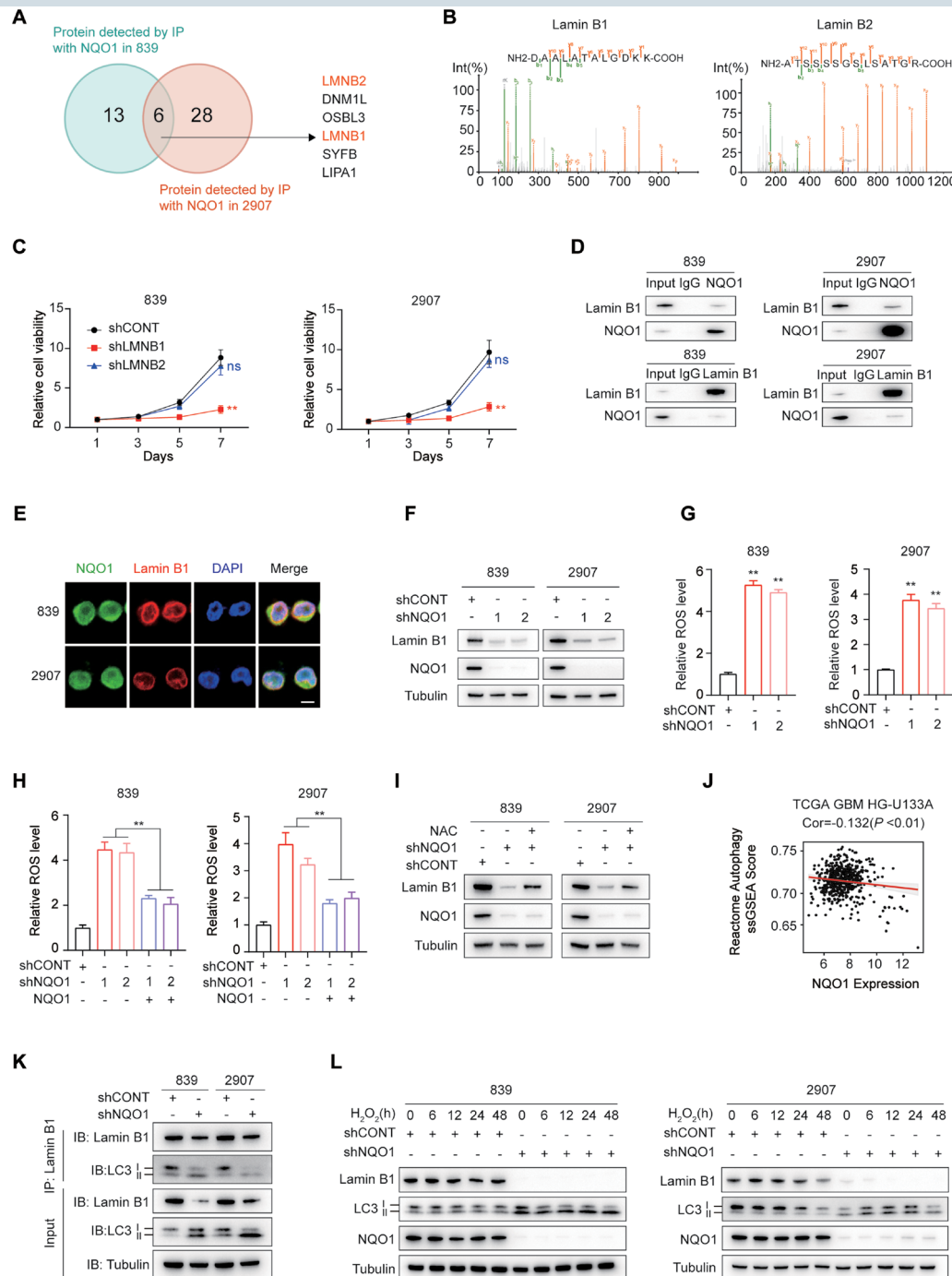


Figure 3. NAD(P)H: quinone oxidoreductase 1 (NQO1) protects against oxidative stress and stabilizes nuclear Lamin B1 in glioblastoma stem cells (GSCs). (A) The Venn diagram illustrates the overlap of proteins identified through immunoprecipitation followed by mass spectrometry using an anti-NQO1 antibody from cell lysates of 839 and 2907 GSCs. (B) Representative peptides of Lamin B1 and Lamin B2 identified by immunoprecipitation followed by mass spectrometry using anti-NQO1 antibody from cell lysates in 839 GSCs. (C) Relative cell viability of 839 and 2907 GSCs expressing shCONT, shLMNB1, or shLMNB2 was measured using a CellTiter-Glo assay. Data are presented as mean \pm SD from 6 independent experiments (** $P < .01$). (D) Immunoblot of immunoprecipitation with anti-NQO1 and anti-Lamin B1 antibody in 839 and 2907 GSCs. Nonspecific IgG serves as the control. (E) Immunofluorescence image of NQO1 and Lamin B1 expression in 839 and 2907 GSCs. Scale bar, 10 μ m. (F) Immunoblot analysis of NQO1 and Lamin B1 protein levels in 839 and 2907 GSCs expressing shCONT, shNQO1-1, or shNQO1-2. (G) Quantification of reactive oxygen species (ROS) level in 839 and 2907 GSCs expressing shCONT, shNQO1-1 and shNQO1-2. Data are presented as mean \pm SD from 6 independent experiments. ** $P < .01$. (H) Quantification of ROS level in 839 and 2907 GSCs expressing shCONT, shNQO1-1, shNQO1-2, shNQO1-1 with overexpression of NQO1, and shNQO1-2 with overexpression of NQO1. ** $P < .01$. (I) Immunoblot analysis of NQO1, Lamin B1 protein levels in 839 and 2907 GSCs expressing shCONT, shNQO1, and shNQO1 treated with NAC. (J) The correlation of NQO1 with autophagy in TCGA GBM HG-U133A. (K) Immunoblot of immunoprecipitation with anti-Lamin B1 antibody in 839 and 2907 GSCs. (L) Immunoblot analysis of NQO1, Lamin B1 and LC3 protein levels in 839 and 2907 GSCs expressing shCONT treated with H2O2, and shNQO1 treated with H2O2 over the indicated time course.

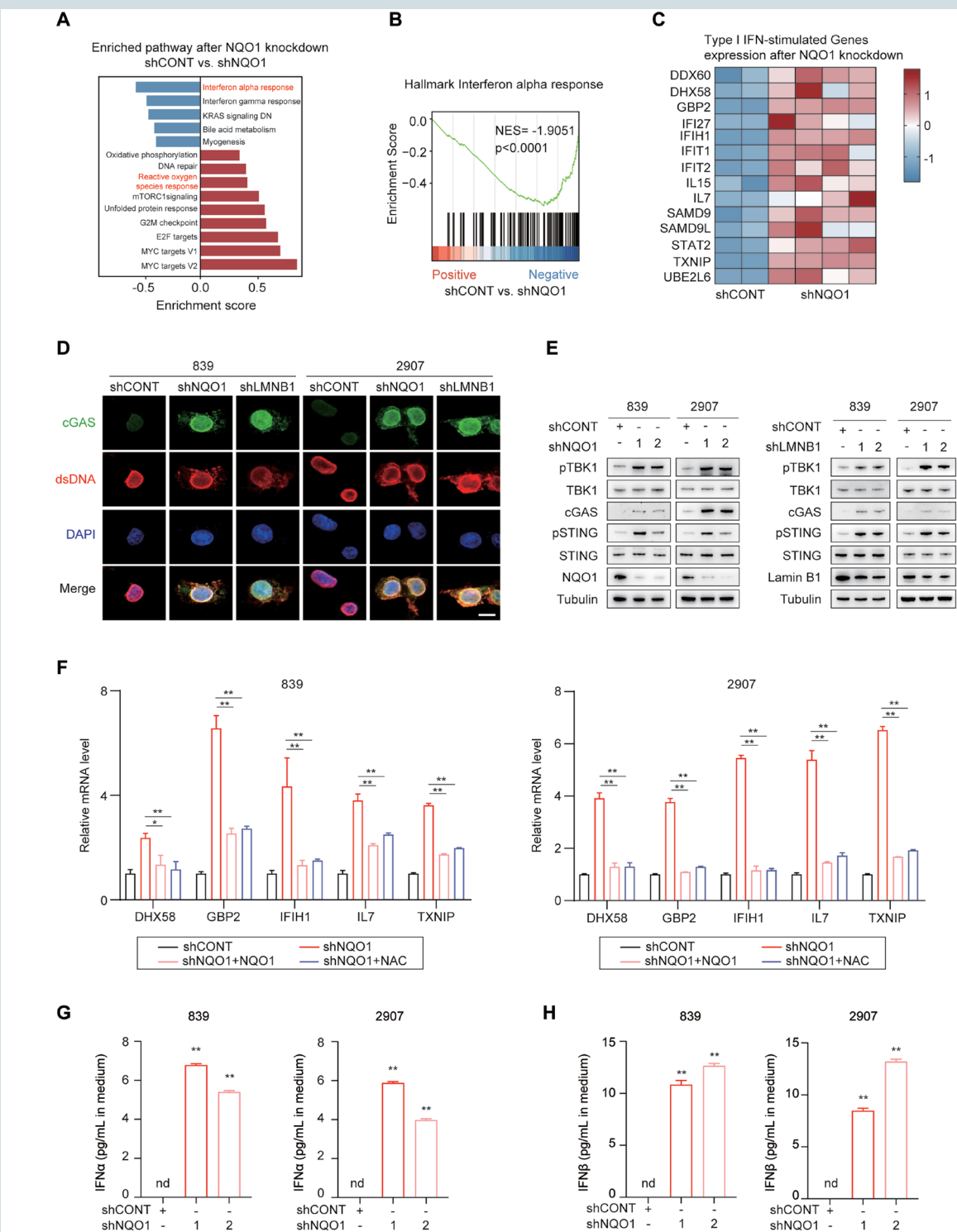


Figure 4. NAD(P)H: quinone oxidoreductase 1 (NQO1) inhibits cGAS-type I interferon signaling. (A) Bar plot showing gene set enrichment analysis (GSEA) for Hallmark gene sets after the knockout of *NQO1*, as determined by RNA sequencing. (B) GSEA scores calculated from RNA sequencing data indicate that *NQO1* expression is negatively correlated with the transcriptional signature of the Interferon alpha response. (C) Heatmap illustrates the expression of upregulated type I interferon-stimulated genes following *NQO1* knockdown in RNA sequencing. (D) Immunofluorescence image of cGAS and dsDNA expression in glioblastoma stem cells (GSCs) expressing shCONT, shNQO1, and shLMNB1. Scale bar, 10 μm. (E) Protein level of TBK1, pTBK1, cGAS, STING, pSTING, and NQO1 in 839 and 2907 GSCs expressing shCONT, shNQO1 (left), or shLMNB1 (right). (F) Quantitative RT-PCR analysis of mRNA levels of type I interferon-stimulated genes in 839 (left) and 2907 (right) GSCs expressing shCONT, shNQO1, shNQO1 with overexpression of *NQO1*, and shNQO1 treated with NAC. ***P* < .01. (G) Quantification of IFNα levels in 839 and 2907 GSCs expressing shCONT, shNQO1-1, and shNQO1-2. *n* = 3, ***P* < .01. (H) Quantification of IFNβ levels in 839 and 2907 GSCs expressing shCONT, shNQO1-1, and shNQO1-2. *n* = 3, ***P* < .01.

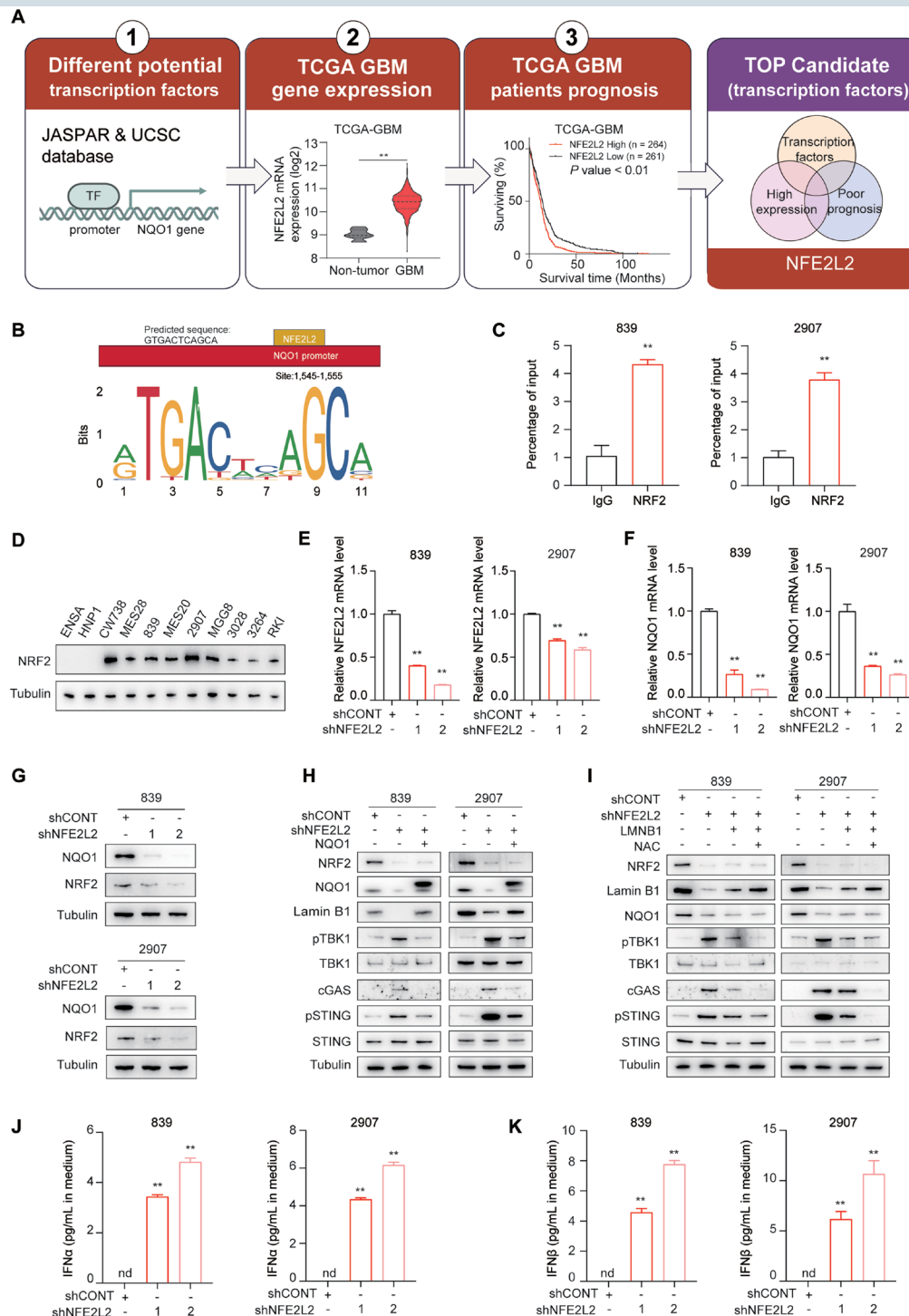


Figure 5. NRF2 transcriptionally regulates NAD(P)H: quinone oxidoreductase 1 (NQO1), inhibiting cGAS-STING signaling. (A) Diagram depicting the screening strategy to identify the overlap of *NQO1* transcription factors with high expression and poor prognosis in TCGA-GBM database. (B) The predicted NRF2 binding site is shown in the promoter region of *NQO1*. (C) ChIP-PCR assay of the enrichment of NRF2 on the *NQO1* promoter region. ** $P < .01$. (D) Protein levels of NRF2 in NSCs (n = 2) and glioblastoma stem cells (GSCs) (n = 9). (E) Quantitative RT-PCR of *NFE2L2* mRNA levels in 839 and 2907 GSCs expressing shCONT, shNFE2L2-1, and shNFE2L2-2. ** $P < .01$. (F) Quantitative RT-PCR of *NQO1* mRNA levels in 839 and 2907 GSCs expressing shCONT, shNFE2L2-1, and shNFE2L2-2. ** $P < .01$. (G) Protein levels of NRF2, NQO1, Lamin B1, TBK1, pTBK1, GAS, STING and pSTING in 839 and 2907 GSCs expressing shCONT, shNFE2L2-1, and shNFE2L2-2. (H) Protein levels of NRF2, NQO1, Lamin B1, TBK1, pTBK1, GAS, STING and pSTING in 839 and 2907 GSCs expressing shCONT, shNFE2L2, shNFE2L2 with overexpression of *NQO1*. (I) Protein levels of NRF2, NQO1, Lamin B1, TBK1, pTBK1, GAS, STING, and pSTING in 839 and 2907 GSCs expressing shCONT, shNFE2L2, shNFE2L2 with overexpression of *LMNB1*, shNFE2L2 with overexpression of *LMNB1* treated with NAC. (J) Quantification of IFN α levels in 839 and 2907 GSCs expressing shCONT, shNFE2L2-1, and shNFE2L2-2. n = 3, ** $P < .01$. (K) Quantification of IFN β levels in 839 and 2907 GSCs expressing shCONT, shNFE2L2-1, and shNFE2L2-2. n = 3, ** $P < .01$.

Silencing *NFE2L2* increased the gene levels of IFN signaling, such as *DHX58*, *GBP2*, *IFIH1*, *IL7*, and *TXNIP* (Supplementary Figure S6A). ELISA assays verified the increased levels of interferon alpha and interferon beta production in supernatant after knocking down *NFE2L2* in GSCs (Figure 5J and K). Therefore, NRF2 transcriptionally regulated *NQO1* inhibits downstream cGAS-STING signaling.

Therapeutic Efficacy of β -Lapachone Combined with Programmed Death-1 Antibody and Remodeling the TME in Glioblastoma

To establish the pharmacologic inhibition of NQO1 by its specific antagonist, which could impact GSCs and inhibit GBM tumor growth. We selected β -lapachone for our pre-clinical study, since β -lapachone is metabolized by NQO1, resulting in the generation of ROS.³⁸ Treatment of GSCs (MES28, RKI, 3028, 839, 2907) with the β -lapachone inhibited GSC proliferation at submicromolar concentrations in vitro (Figure 6A). Given our data demonstrated that NQO1 inhibits cGAS-STING signaling, which is a critical pathway for immune activation through the production of Type I interferon and T cell activation, we designed a preclinical trial using an immunocompetent orthotopic xenograft model. Nqo1-silenced murine CT-2A cells were transplanted into immunocompetent C57BL/6J mice. Mice bearing CT-2A with *Nqo1* knockdown exhibited prolonged tumor latency and reduced tumor volumes compared with those transduced with a control shRNA (Figure 6B-D, Supplementary Figure S7A-C). We further profiled the immune cell compartments by flow cytometry, systematically quantifying the major immune cell populations, and observed that CD8⁺ T cells increased significantly in abundance after β -lapachone treatment, whereas CD4⁺ T cells showed no significant decrease. TAMs, MDSCs, and Treg cells showed a modest, nonsignificant decrease (Supplementary Figure S7D-I).

To further investigate the potential for combinatorial therapeutic efficacy in vivo, we implanted CT-2A transduced with luciferase into the brains of immunocompromised mice to evaluate the impact of targeting NQO1 and programmed death-1 (PD-1) on tumor growth. Tumor-bearing mice underwent treatment with vehicle control, anti-PD-1 (200 μ g with intraperitoneal injection every 5 days), β -lapachone (22 mg/kg with intraperitoneal injection every 2 days), or the combination of β -lapachone (22 mg/kg with intraperitoneal injection every 2 days) and anti-PD-1 (200 μ g with intraperitoneal injection every 5 days). Combined targeting of NQO1 and PD-1 inhibitor treatment significantly enhanced overall survival and reduced tumor volume compared with either monotherapy or the vehicle control group in intracranial xenograft models (Figure 6E-H, Supplementary Figure S7J). Moreover, we examined CD8⁺ T cells and IFN- γ positive cells with the individual and combinatorial therapeutic efficacy. CD8⁺ T cell exhibited enhanced infiltration and activity after the combined treatment of anti-PD-1 antibody and β -lapachone, as measured by flow cytometry and immunohistochemistry, suggesting that low CD8⁺ T cell infiltration was induced by the expression of NQO1 under the condition of GSCs against OS (Figure 6I and J, Supplementary Figure S8A and B). We analyzed the TCGA and several GBM datasets and revealed that NQO1 informed poor prognosis in

GBM patients (Figure 6K, Supplementary Figure S8C). Collectively, our data suggested that targeting NQO1 augments the anti-tumor efficacy of anti-PD-1, providing a new therapeutic approach to improve glioblastoma therapy.

Discussion

The establishment of an immunosuppressive environment is closely linked to OS within the TME, which is characterized by elevated levels of ROS.³⁹ GSCs adapt to and maintain redox homeostasis to counteract the heightened levels of ROS, facilitating radiotherapeutic resistance.⁴⁰ NQO1 has been associated with regulating various solid tumors, promoting tumor cell metabolism, glycolysis, and redox homeostasis.^{41,42} However, the role of NQO1 in the context of GSCs and the TME in GBM has not been clearly defined. In this study, we found NQO1 is overexpressed in GSCs compared with NSCs and validated its essential role in GSCs and non-GSC tumor cells to address GBM microenvironment heterogeneity. NQO1 acts as a critical regulator of GSC proliferation and self-renewal and helps confer resistance to OS and maintains nuclear integrity through Lamin B1, inhibiting cGAS-type I interferon signaling, which in turn promotes an immunosuppressive TME (Figure 6L). Pharmacological inhibition of NQO1 in conjunction with anti-PD-1 therapy, demonstrated significant therapeutic potential against GSCs and TME, offering new strategies to enhance treatment options for glioblastoma.

Previous studies described a small-molecule inhibitor that binds NQO1 and GSTP1 with high affinity and selectivity, induces apoptosis in GBM, and specifically suppresses the growth of cell lines and primary GBM.⁴³ Zhong identified an NQO1-dependent form of necrosis.⁴⁴ However, the role of NQO1 in modulating nuclear lamina function remains poorly understood. The nuclear lamina constitutes a fibrillar network positioned beneath the nuclear envelope, composed of 4 isoforms of nuclear lamins—Lamin B1, B2, Lamin A and C—and their associated proteins.⁴⁵ B-type lamins are predominantly localized to the nuclear periphery, in close apposition to the inner nuclear membrane.⁴⁶ The nuclear lamina is essential for maintaining nuclear shape, and its dysregulation causes the accumulation of cytosolic chromatin fragments. In this study, we found that NQO1 prevents ROS generation and induces OS resistance while maintaining the stability of nuclear Lamin B1 in GSCs. GSCs exhibit heightened sensitivity and diminished cell viability against OS upon Lamin B1 deficiency compared to Lamin B2 deficiency. Silencing *NQO1* or *LMNB1* enhanced nuclear translocation, as indicated by the increased presence of dsDNA in the cytoplasm. Existing studies are limited to the effect of NQO1 on ROS-induced apoptosis, promoting radioresistance and chemoresistance.⁴⁷ Interestingly, our data observed that inhibiting NQO1 activates OS and induces the degradation of Lamin B1 via the autophagy pathway, which further activates the downstream cGAS-STING and type I interferon signaling.

NRF2 is a critical transcription factor that plays a pivotal role in maintaining cellular redox homeostasis and defending against OS.⁴⁸ It modulates the expression of antioxidant enzymes, including heme oxygenase-1 (HO-1) and NQO1, which helps reduce OS.⁴⁹ NRF2 enhances the survival of

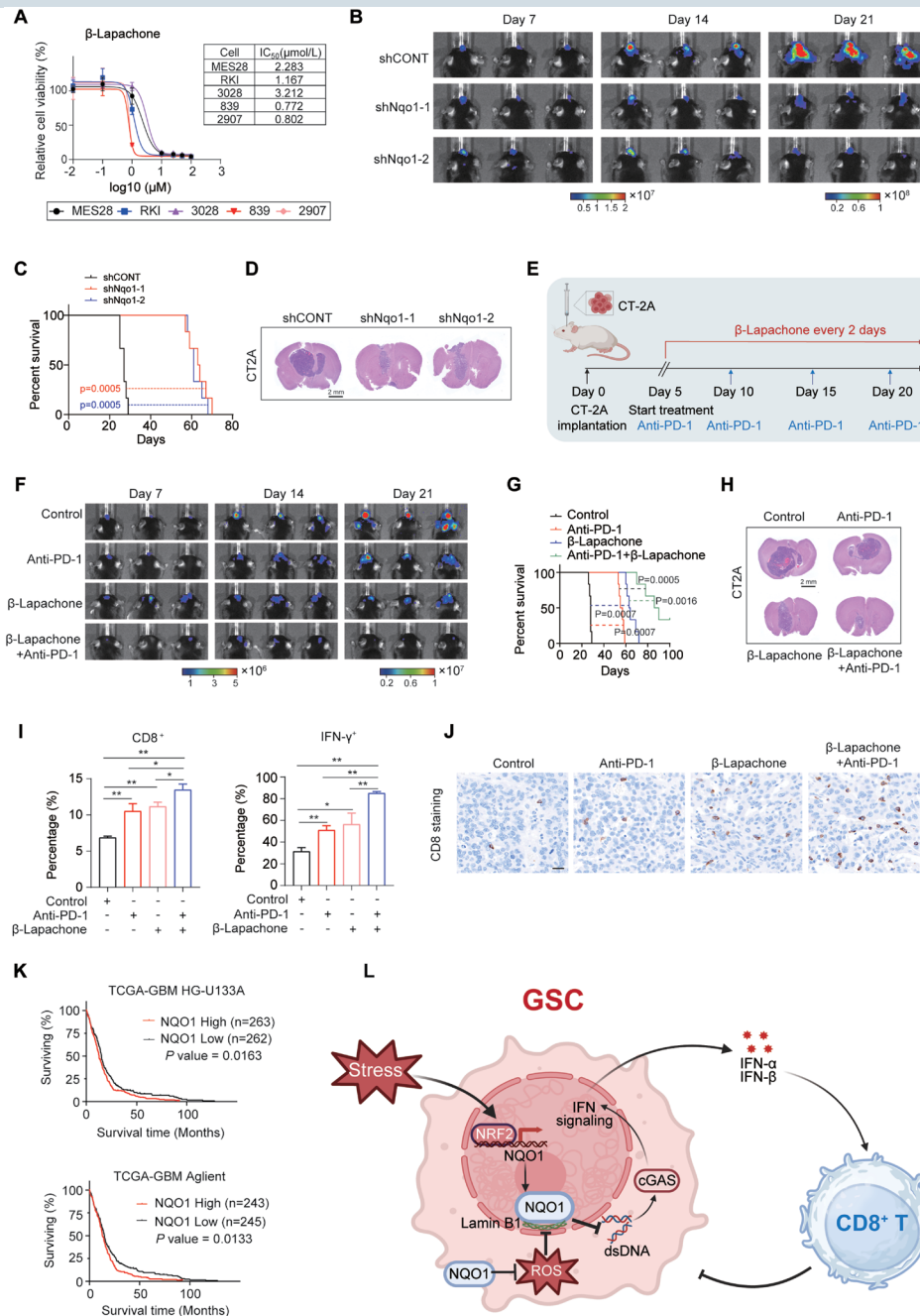


Figure 6. Therapeutic efficacy of β -lapachone combined with PD-1 antibody in inhibiting tumor growth. (A) Dose-response curves for β -lapachone stimulation and IC₅₀ determination in glioblastoma stem cells (GSCs) (MES28, RKI, 3028, 839, 2907), as measured by a CellTiter-Glo assay. Data are presented as mean \pm SD from 6 independent experiments. (B) In vivo bioluminescent imaging of tumor growth, conducted on C57BL/6J mice bearing CT2A-derived intracranial tumors expressing shCONT, shNQO1-1, or shNQO1-2 on days 7, 14, and 21. (C) Kaplan-Meier survival curves for C57BL/6J mice bearing glioblastoma xenografts derived from CT2A expressing shCONT, shNQO1-1, or shNQO1-2 ($n = 6$). P values were determined by the log-rank test. (D) Representative images of H&E staining of mouse brains were collected on day 21 after the transplantation of CT2A, expressing shCONT, shNQO1-1, or shNQO1-2. Scale bar, 2 mm. (E) Schematic illustrating the implantation of CT2A into the brains of C57BL/6J mice. C57BL/6J mice were treated with anti-PD-1, β -lapachone, or the combination treatment. Created in BioRender. <https://BioRender.com/3mft6u7>. (F) In vivo bioluminescent imaging of tumor growth conducted in C57BL/6J mice bearing CT2A-derived intracranial tumors with anti-PD-1, β -lapachone, or the combination treatment, assessed on days 7, 14, and 21. (G) Kaplan-Meier survival curves for C57BL/6J mice bearing glioblastoma xenografts derived from CT2A treated with anti-PD-1, β -lapachone or the combination treatment. $n = 6$. P values were determined by the log-rank test. (H) Representative images of H&E staining of mouse brain collected on day 21 after transplantation of CT2A treated with anti-PD-1, β -lapachone or the combination treatment. Scale bar, 2 mm. (I) Flow cytometry quantification of CD8⁺ T cells (left) and IFN- γ ⁺ CD8⁺ T cells (right) in C57BL/6J mice bearing glioblastoma xenografts derived from CT2A treated with anti-PD-1, β -lapachone or the combination treatment, $n = 3$. Data were presented as the mean \pm SD. * $P < .05$, ** $P < .01$. (J) Representative immunohistochemical (IHC) staining of CD8⁺ T cells from indicated tumors. Scale bar, 20 μ m. (K) Kaplan-Meier survival analysis of NQO1 by the median of different glioma data sets, including TCGA GBM HG-U133A and TCGA GBM Aglient. (L) A schematic diagram illustrating NQO1-mediated resistance to oxidative stress and remodeling of the TME in GBM. Created in BioRender. <https://BioRender.com/vw8klad>.

tumor cells under hypoxic conditions by upregulating the expression of hypoxia-inducible factor-1 α (HIF-1 α) and vascular endothelial growth factor.⁵⁰ Our study demonstrated that NRF2 transcriptionally regulated NQO1 inhibits cGAS-STING signaling and maintains the immunosuppressive TME.

β -Lapachone demonstrates pronounced cytotoxic effects on neoplasms by triggering immunogenic cell death, augmenting tumor immunogenicity, effectively ablating immunocompetent murine tumors, and augmenting the infiltration of neutrophils into the TME.⁵¹ It is noteworthy that β -lapachone injection (ARQ 501) has undergone several cancer treatment clinical trials, including NCT00102700, NCT00310518, NCT00358930, NCT00524524, NCT00622063, and NCT00099190.^{52,53} And β -lapachone prodrug (ARQ 761) has also completed clinical trials (NCT01502800).⁵⁴ These trials highlight the potential of β -lapachone as an anticancer agent, primarily through its selective targeting of cancer cells via the NQO1 pathway. Our data provide definitive evidence that β -lapachone acts synergistically with anti-PD-1 immunotherapy in GBM tumors, enhancing CD8⁺ T-cell inflammation. This indicates that targeting NQO1 enhances the anti-tumor efficacy of anti-PD-1 therapy and offers a novel therapeutic strategy to optimize glioblastoma treatment outcomes.

In conclusion, our results indicate that NQO1 serves as both an antioxidant stress response regulator and a factor in maintaining GSCs within an immunosuppressive TME. NQO1 helps prevent OS, particularly by reducing ROS levels, which supports the stability of nuclear Lamin B1. This stability, in turn, inhibits cGAS-STING signaling and type I interferon pathways, contributing to the remodeling of the immunosuppressive TME. Additionally, the transcription factor NRF2 regulates NQO1 and inhibits cGAS-type I interferon signaling. This study identifies new therapeutic targets for clinical treatment at both the cell-autonomous and cell-extrinsic levels. Targeting NQO1 and its downstream signaling effectors, such as β -lapachone and anti-PD-1, may offer effective strategies for treating GBM.

Supplementary Material

Supplementary material is available online at Neuro-Oncology (<https://academic.oup.com/neuro-oncology>).

Keywords

glioblastoma | glioblastoma stem cells | NQO1 | oxidative stress | tumor microenvironment

Author Contributions

Conception and design: Q.Z., Y.L., and C.L. Collection and assembly of data: T.K., Z.J., C.L., G.C., and K.S. Data analysis and interpretation: Y.L., D.S., Q.L., D.L., and H.Y. Manuscript writing: Q.Z. and Y.L. Revision and final approval of manuscript: all authors. Accountable for all aspect of the study: all authors.

Conflict of Interest Statement

The authors declare no competing interests.

Funding

This research was supported by the National Natural Science Foundation of China (grants 82573312 to Q.Z., 82525047 to X.W., and 82403659 to C.L.); the Clinical Research Foundation for the Prevention and Treatment of Collaborative Innovation Center for Cancer Personalized Medicine of Nanjing Medical University (grants 2024CICCPMHR036 to Q.Z. and 2024CICCPMHR015 to X.W.); the Jiangsu Province High-Level Hospital Pairing Assistance Construction Funds (grant zdlyg05 to K.Y.); the Research Personnel Cultivation Programme of Zhongda Hospital Southeast University (grant CZXM-GSP-RC-152 to K.Y.), the Medical Science and Technology Development Foundation of Nanjing (grant ZKX22041 to K.Y.), and Natural Science Foundation of Jiangsu Province (grant BK20241130 to C.L.).

Data Availability

Raw data and processed data of RNA-seq presented were deposited in the GEO database (GSE301343). All data accessed from external sources and prior publications have been referenced in the text and corresponding figure legends. Additional data will be made available upon request.

Affiliations

Ministry of Education Key Laboratory of Model Animals for Disease Study, Model Animal Research Center, Medical School of Nanjing University, National Resource Center for Mutant Mice, Nanjing, Jiangsu, China (Y.L., C.L.); National Health Commission Key Laboratory of Antibody Techniques, Department of Cell Biology, Jiangsu Key Laboratory of Molecular Targets and Intervention for Metabolic Diseases, School of Basic Medical Sciences, Nanjing Medical University, Nanjing, Jiangsu, China (T.K., Z.J., G.C., H.Y., D.S., Q.L., D.L., H.Y., D.G., J.G., W.G., F.L., X.W., L.S. Q.Z.); Institute for Brain Tumors, Jiangsu Key Laboratory of Cancer Biomarkers, Prevention, and Treatment, Collaborative Innovation Center for Cancer Personalized Medicine, Nanjing Medical University, Nanjing, Jiangsu, China (C.L., D.G., J.G., Q.W., J.Z., X.Q., X.W., Q.Z.); Department of Neurosurgery, The First Affiliated Hospital of Nanjing Medical University, Nanjing, Jiangsu, China (C.L., K.S., Z.S., J.Z., Y.Y., X.W.); Department of Neurology and Herbert Irving Comprehensive Cancer Center, Columbia University, New York, New York, USA (D.D.); The Second Clinical Medical School, Nanjing Medical University, Nanjing, Jiangsu, China (F.J.); The Third Affiliated Hospital of Nanjing Medical University, Changzhou Medical Center, Changzhou, Jiangsu, China (W.G., L.S.); Department of Pathology and Cell Biology, Columbia University Irving Medical Center, New York, New York, USA (Z.Z.); College of Biomedicine and Health & College of Life Science and Technology, Huazhong Agricultural University, Wuhan, Hubei, China (W.T.);

Neurosurgery Department, Institute of Neuroscience, Lianyungang Clinical College of Nanjing Medical University, The First People's Hospital of Lianyungang, The First Affiliated Hospital of Kangda College of Nanjing Medical University, Lianyungang, China (J.L.); Science Island Branch of Graduate, University of Science and Technology of China, Hefei, China (Z.Z.); Department of Radiation Oncology, Holden Comprehensive Cancer Center, Iowa Neuroscience Institute, University of Iowa, Iowa City, Iowa, USA (Ka.Y.); Lineberger Comprehensive Cancer Center, University of North Carolina, Chapel Hill, North Carolina, USA (J.N.R.); Department of Neurosurgery, Zhongda Hospital, Southeast University, Nanjing, Jiangsu, China (Ku.Y.); State Key Laboratory of Reproductive Medicine and Offspring Health, China International Joint Research Center on Environment and Human Health, Center for Global Health, School of Public Health, Gusu School, Nanjing Medical University, Nanjing, Jiangsu, China (C.L.)

References

1. Tan AC, Ashley DM, López GY, Malinzak M, Friedman HS, Khasraw M. Management of glioblastoma: state of the art and future directions. *CA Cancer J Clin.* 2020;70:299-312. <https://doi.org/10.3322/caac.21613>
2. Miller KD, Ostrom QT, Kruchko C, et al. Brain and other central nervous system tumor statistics, 2021. *CA Cancer J Clin.* 2021;71:381-406. <https://doi.org/10.3322/caac.21693>
3. Ostrom QT, Price M, Neff C, et al. CBTRUS statistical report: primary brain and other central nervous system tumors diagnosed in the United States in 2015-2019. *Neuro Oncol.* 2022; 24:v1-v95. <https://doi.org/10.1093/neuonc/noac202>
4. Pouyan A, Ghorbanlo M, Eslami M, et al. Glioblastoma multiforme: insights into pathogenesis, key signaling pathways, and therapeutic strategies. *Mol Cancer.* 2025;24:58. <https://doi.org/10.1186/s12943-025-02267-0>
5. Gilbertson RJ, Rich JN. Making a tumour's bed: glioblastoma stem cells and the vascular niche. *Nat Rev Cancer.* 2007;7:733-736. <https://doi.org/10.1038/nrc2246>
6. Lathia JD, Mack SC, Mulkearns-Hubert EE, Valentim CL, Rich JN. Cancer stem cells in glioblastoma. *Genes Dev.* 2015;29:1203-1217. <https://doi.org/10.1101/gad.261982.115>
7. Lan X, Jorg DJ, Cavalli FMG, et al. Fate mapping of human glioblastoma reveals an invariant stem cell hierarchy. *Nature.* 2017;549:227-232. <https://doi.org/10.1038/nature23666>
8. Prager BC, Xie Q, Bao S, Rich JN. Cancer stem cells: the architects of the tumor ecosystem. *Cell Stem Cell.* 2019;24:41-53. <https://doi.org/10.1016/j.stem.2018.12.009>
9. Dapash M, Hou D, Castro B, Lee-Chang C, Lesniak MS. The interplay between glioblastoma and its microenvironment. *Cells.* 2021;10:2257. <https://doi.org/10.3390/cells10092257>
10. Liu Y, Zhou F, Ali H, Lathia JD, Chen P. Immunotherapy for glioblastoma: current state, challenges, and future perspectives. *Cell Mol Immunol.* 2024;21:1354-1375. <https://doi.org/10.1038/s41423-024-01226-x>
11. Hayes JD, Dinkova-Kostova AT, Tew KD. Oxidative stress in cancer. *Cancer Cell.* 2020;38:167-197. <https://doi.org/10.1016/j.ccell.2020.06.001>
12. Zheng Y, Sun J, Luo Z, Li Y, Huang Y. Emerging mechanisms of lipid peroxidation in regulated cell death and its physiological implications. *Cell Death Dis.* 2024;15:859. <https://doi.org/10.1038/s41419-024-07244-x>
13. Sajadimajd S, Khazaei M. Oxidative stress and cancer: the role of Nrf2. *Curr Cancer Drug Targets.* 2018;18:538-557. <https://doi.org/10.2174/1568009617666171002144228>
14. Glorieux C, Liu S, Trachootham D, Huang P. Targeting ROS in cancer: rationale and strategies. *Nat Rev Drug Discov.* 2024;23:583-606. <https://doi.org/10.1038/s41573-024-00979-4>
15. Cheng X, Geng F, Pan M, et al. Targeting DGAT1 ameliorates glioblastoma by increasing fat catabolism and oxidative stress. *Cell Metab.* 2020;32:229-242.e8. <https://doi.org/10.1016/j.cmet.2020.06.002e228>
16. Ye Z, Ai X, Yang K, et al. Targeting microglial metabolic rewiring synergizes with immune-checkpoint blockade therapy for glioblastoma. *Cancer Discov.* 2023;13:974-1001. <https://doi.org/10.1158/2159-8290.CD-22-0455>
17. Nowacka A, Śniegocki M, Ziolkowska E. Oxidative stress and antioxidants in glioblastoma: mechanisms of action, therapeutic effects and future directions. *Antioxidants (Basel).* 2025;14:1121. <https://doi.org/10.3390/antiox14091121>
18. Sun G, Cao Y, Qian C, et al. Romo1 is involved in the immune response of glioblastoma by regulating the function of macrophages. *Aging (Albany NY).* 2020;12:1114-1127. <https://doi.org/10.18632/aging.102648>
19. Yuan Z, Wang X, Qin B, et al. Targeting NQO1 induces ferroptosis and triggers anti-tumor immunity in immunotherapy-resistant KEAP1-deficient cancers. *Drug Resist Updat.* 2024;77:101160. <https://doi.org/10.1016/j.drug.2024.101160>
20. Li X, Liu ZA-O, Zhang A, et al. NQO1 targeting prodrug triggers innate sensing to overcome checkpoint blockade resistance. *Nat Commun.* 2019;10:3251. <https://doi.org/10.1038/s41467-019-11238-1>
21. Luo S, Lei K, Xiang D, Ye KA-O. NQO1 is regulated by PTEN in glioblastoma, mediating cell proliferation and oxidative stress. *Oxid Med Cell Longev.* 2018;2018:9146528. <https://doi.org/10.1155/2018/9146528>
22. Ma Y, Kong J, Yan G, et al. NQO1 overexpression is associated with poor prognosis in squamous cell carcinoma of the uterine cervix. *BMC Cancer.* 2014;14:414. <https://doi.org/10.1186/1471-2407-14-414>
23. Zheng L, Yang S, Xu R, et al. NQO1 drives glioblastoma cell aggressiveness through EMT induction via the PI3K/Akt/mTOR/Snail pathway. *Int J Oncol.* 2023;63:110. <https://doi.org/10.3892/ijo.2023.5558>
24. Lei K, Xia Y, Wang XC, Ahn EH, Jin L, Ye K. C/EBPβ mediates NQO1 and GSTP1 anti-oxidative reductases expression in glioblastoma, promoting brain tumor proliferation. *Redox Biol.* 2020;34:101578. <https://doi.org/10.1016/j.redox.2020.101578>
25. Wang X, Huang Z, Wu Q, et al. MYC-regulated mevalonate metabolism maintains brain Tumor-Initiating cells. *Cancer Res.* 2017;77:4947-4960. <https://doi.org/10.1158/0008-5472.CAN-17-0114>
26. Flavahan WA, Wu Q, Hitomi M, et al. Brain tumor initiating cells adapt to restricted nutrition through preferential glucose uptake. *Nat Neurosci.* 2013;16:1373-1382. <https://doi.org/10.1038/nn.3510>
27. Wang X, Prager BC, Wu Q, et al. Reciprocal signaling between glioblastoma stem cells and differentiated tumor cells promotes malignant progression. *Cell Stem Cell.* 2018;22:514-528.e5. <https://doi.org/10.1016/j.stem.2018.03.01115>
28. Hu Y, Smyth GK. ELDA: extreme limiting dilution analysis for comparing depleted and enriched populations in stem cell and other assays. *J Immunol Methods.* 2009;347:70-78. <https://doi.org/10.1016/j.jim.2009.06.008>
29. Patro R, Duggal G, Love MI, Irizarry RA, Kingsford C. Salmon provides fast and bias-aware quantification of transcript expression. *Nat Methods.* 2017;14:417-419. <https://doi.org/10.1038/nmeth.4197>
30. Sonesson C, Love MI, Robinson MD. Differential analyses for RNA-seq: transcript-level estimates improve gene-level inferences. *F1000Res.* 2015;4:1521. <https://doi.org/10.12688/f1000research.7563.1>

31. Love MI, Huber W, Anders S. Moderated estimation of fold change and dispersion for RNA-seq data with DESeq2. *Genome Biol.* 2014;15:550. <https://doi.org/10.1186/s13059-014-0550-8>
32. Ravi VM, Will P, Kueckelhaus J, et al. Spatially resolved multi-omics deciphers bidirectional tumor-host interdependence in glioblastoma. *Cancer Cell.* 2022;40:639-655.e13. <https://doi.org/10.1016/j.ccell.2022.05.009>
33. Li D, Cui G, Yang K, et al. Inhibiting macrophage-derived lactate transport restores cGAS-STING signalling and enhances antitumour immunity in glioblastoma. *Nat Cell Biol.* 2026. <https://doi.org/10.1038/s41556-025-01839-y>
34. Mack SC, Singh I, Wang X, et al. Chromatin landscapes reveal developmentally encoded transcriptional states that define human glioblastoma. *J Exp Med.* 2019;216:1071-1090. <https://doi.org/10.1084/jem.2019019630948495>
35. Ravi VM, Will P, Kueckelhaus J, et al. Spatially resolved multi-omics deciphers bidirectional tumor-host interdependence in glioblastoma. *Cancer Cell.* 2022;40:639-655.e13. <https://doi.org/10.1016/j.ccell.2022.05.00935700707>
36. Molenberghs F, Verschuuren M, Vandeweyer L, et al. Lamin B1 curtails early human papillomavirus infection by safeguarding nuclear compartmentalization and autophagic capacity. *Cell Mol Life Sci.* 2024;81:141. <https://doi.org/10.1007/s00018-024-05194-3>
37. Liu S, Yao S, Yang H, Liu S, Wang Y. Autophagy: regulator of cell death. *Cell Death Dis.* 2023;14:648. <https://doi.org/10.1038/s41419-023-06154-8>
38. Dai Y, Min Y, Zhou L, et al. Brain-targeting redox-sensitive micelles for codelivery of TMZ and beta-lapachone for glioblastoma therapy. *Nanomedicine.* 2024;61:102772. <https://doi.org/10.1016/j.nano.2024.102772>
39. Papavassiliou K, Sofianidi A, Gogou V, Papavassiliou A. Leveraging the ROS-TME axis for cancer treatment. *Antioxidants (Basel).* 2024;13:1365. <https://doi.org/10.3390/antiox13111365>
40. Huang H, Zhang S, Li Y, et al. Suppression of mitochondrial ROS by prohibitin drives glioblastoma progression and therapeutic resistance. *Nat Commun.* 2021;12:3720. <https://doi.org/10.1038/s41467-021-24108-6>
41. Wang X, Liu Y, Han A, et al. The NQO1/p53/SREBP1 axis promotes hepatocellular carcinoma progression and metastasis by regulating snail stability. *Oncogene.* 2022;41:5107-5120. <https://doi.org/10.1038/s41388-022-02477-6>
42. Oh ET, Kim JW, Kim JM, et al. NQO1 inhibits proteasome-mediated degradation of HIF-1alpha. *Nat Commun.* 2016;7:13593. <https://doi.org/10.1038/ncomms13593>
43. Lei K, Gu X, Alvarado AG, et al. Discovery of a dual inhibitor of NQO1 and GSTP1 for treating glioblastoma. *J Hematol Oncol.* 2020;13:141. <https://doi.org/10.1186/s13045-020-00979-y>
44. Zhong B, Yu J, Hou Y, et al. A novel strategy for glioblastoma treatment by induction of noptosis, an NQO1-dependent necrosis. *Free Radic Biol Med.* 2021;166:104-115. <https://doi.org/10.1016/j.freeradbiomed.2021.02.014>
45. Wang TC, Abolghasemzade S, McKee BP, et al. Matrix stiffness drives drop like nuclear deformation and lamin a/C tension-dependent YAP nuclear localization. *Nat Commun.* 2024;15:10151. <https://doi.org/10.1038/s41467-024-54577-4>
46. Hwang I, Uchida H, Dai Z, et al. Cellular stress signaling activates type-I IFN response through FOXO3-regulated lamin posttranslational modification. *Nat Commun.* 2021;12:640. <https://doi.org/10.1038/s41467-020-20839-0>
47. Xue W, Wang T, Tian WJ, Pang SQ, Zhang HF, Jia WD. NQO1 mediates lenvatinib resistance by regulating ROS-induced apoptosis in hepatocellular carcinoma. *Curr Med Sci.* 2024;44:168-179. <https://doi.org/10.1007/s11596-023-2804-8>
48. Tang L, He D, Su B. Nrf2: a critical participant in regulation of apoptosis, ferroptosis, and autophagy in gastric cancer. *Acta Histochem.* 2024;126:152203. <https://doi.org/10.1016/j.acthis.2024.152203>
49. Dodson M, Castro-Portuguez R, Zhang DD. NRF2 plays a critical role in mitigating lipid peroxidation and ferroptosis. *Redox Biol.* 2019;23:101107. <https://doi.org/10.1016/j.redox.2019.101107>
50. Almeida Lima K, Osawa IYA, Ramalho MCC, et al. Temozolomide resistance in glioblastoma by NRF2: protecting the evil. *Biomedicines.* 2023;11:1081. <https://doi.org/10.3390/biomedicines11041081>
51. Qadir MI, Iqbal MS, Khan R. Beta-lapachone: a promising anticancer agent with a unique NQO1 specific apoptosis in pancreatic cancer. *Curr Cancer Drug Targets.* 2022;22:537-540. <https://doi.org/10.2174/1568009622666220427121127>
52. Li LS, Bey, EA, Dong Y, et al. Modulating endogenous NQO1 levels identifies key regulatory mechanisms of action of beta-lapachone for pancreatic cancer therapy. *Clin Cancer Res.* 2011;17:275-285. <https://doi.org/10.1158/1078-0432.CCR-10-1983>
53. Zhao L, Miao H, Quan M, et al. beta-Lapachone induces ferroptosis of colorectal cancer cells via NCOA4-mediated ferritinophagy by activating JNK pathway. *Chem Biol Interact.* 2024;389:110866. <https://doi.org/10.1016/j.cbi.2024.110866>
54. Gomes CL, Sales V de AW, Gomes de MC, et al. Beta-lapachone: natural occurrence, physicochemical properties, biological activities, toxicity and synthesis. *Phytochemistry.* 2021;186:112713. <https://doi.org/10.1016/j.phytochem.2021.112713>